Coster-Kronig, fluorescence, and Auger yields of the $_{47}$Ag L subshells measured through synchrotron photoionization

W. Jitschin and R. Stötzel
Fachbereich Mathematik, Naturwissenschaften und Informatik, Fachhochschule Giessen-Friedberg, 35390 Giessen, Germany

T. Papp
Institute of Nuclear Research, Hungarian Academy of Science, P.O. Box 51, 4001 Debrecen, Hungary

M. Sarkar
Saha Institute of Nuclear Physics, 1-AF, Bidhan Nagar, Calcutta 700064, India
(Received 18 September 1998)

The decay of individual L subshell vacancies in $_{47}$Ag has been investigated through selective photoionization by monochromatized synchrotron radiation. By tuning the radiation energy over the L edges, the ionization of particular subshells can be turned off and on. The corresponding subshell ionization cross sections including the subtle structure caused by electron correlations are known from our previous studies. The x-ray fluorescence emitted in the vacancy decay was recorded by a Si (Li) detector. Advanced fitting techniques were employed to extract the intensities of lines originating from different subshells. The extracted line intensities were plotted versus energy of the primary radiation. The relative jumps of the line intensities occurring at the edges directly correspond to the Coster-Kronig yields, whereas the absolute values of the total subshell fluorescence give the fluorescence yields. The following Coster-Kronig yields were obtained: $f_{12}=0.14(3)$, $f_{13}=0.58(5)$, and $f_{23}=0.18(3)$. Adopting the value $\omega_3=0.056(7)$ from literature, the following fluorescence yields are obtained: $\omega_1=0.013(2)$ and $\omega_2=0.067(9)$. The results agree reasonably with theoretical calculations. In particular, the rather large value of f_{13} indicates that the L_1-$L_3M_{4,5}$ Coster-Kronig channel is well allowed. [S1050-2947(99)05005-2]

PACS number(s): 32.50.+d, 32.70.−n, 32.80.Hd, 33.50.−j

I. INTRODUCTION

A vacancy in an inner electron shell created, e.g., by photon or charged particle impact, is rapidly filled up by an electron from a higher-lying (sub)shell. Three different processes compete in the filling: The simplest one is the radiative one-electron decay in which one electron jumps ''down'' and the released energy is emitted as a fluorescence x ray. The other two are nonradiative processes: The so-called Auger process results from the mutual repulsion of two electrons in higher shells that causes one electron to jump down and the other to leave the atom carrying the excess energy as kinetic energy. The so-called Coster-Kronig decay is a special Auger process in which an initial vacancy is transferred to a higher subshell of the *same* shell. The relative probabilities of the various processes of vacancy filling are called (vacancy) yields.

The practical importance of vacancy yields is considerable: For example, they determine the characteristics of the vacancy cascade after inner-shell ionization leading to a multiply ionized ion. The degree of ionization is a decisive parameter for plasmas, e.g., in laboratory ion sources, fusion reactors, and astrophysics. Subshell fluorescent yields are important, e.g., in x-ray fluorescent analysis, radiative energy transport through matter and radiation shielding, medical diagnostics, and astrophysics.

Reliable values of the yields are also of considerable interest for fundamental theory. When Coster-Kronig processes are energetically allowed, they are strong and—in many cases—even the dominant process of vacancy filling. The extraordinary strength of these transitions taxes the limit of the common single-particle picture and a treatment by a perturbative approach. An especially interesting case is the L_1 decay of elements in the vicinity of atomic number $Z \approx 49$ due to the cutoff of the L_1-$L_3M_{4,5}$ Coster-Kronig channel having an extremely large transition rate [1]. When Z is smaller than 48, this channel is energetically allowed and the dominant one, but when Z is larger than 50, it is blocked [2]. In a tabulation of theoretical values, a sharp cutoff has (somewhat arbitrarily) been placed between $Z=49$ and $Z=50$ [3]. A closer look at the energy threshold reveals that the abrupt cutoff is smeared out by the multiplet structure of the final state. Furthermore, when the transition is allowed just above threshold, the emitted electron has tiny kinetic energy and strongly interacts with the remaining ion during its slow escape. The multielectron nature of the interaction provides a challenge for atomic theory. Experimental data indicate, in fact, that the cutoff is not sharp but extends over a certain range $Z=48...50$ [4,5]. Decisive experimental data are needed to settle this problem.

Various experimental methods for measuring L subshell yields are available [6,7]. The $K\alpha$-$L\alpha$ coincidence method provides a powerful tool for a precise measurement of all L_2 and L_3 subshell yields, namely, the fluorescence yields ω_3, ω_2, and the Coster-Kronig yield f_{23}. However, this method is not applicable to L_1 subshell yields. Various experimental methods have been explored to measure L_1 subshell yields, which suffer from different problems. Still, in the early 1980s, rather few experimental data on L_1 yields with only

 ©1999 The American Physical Society

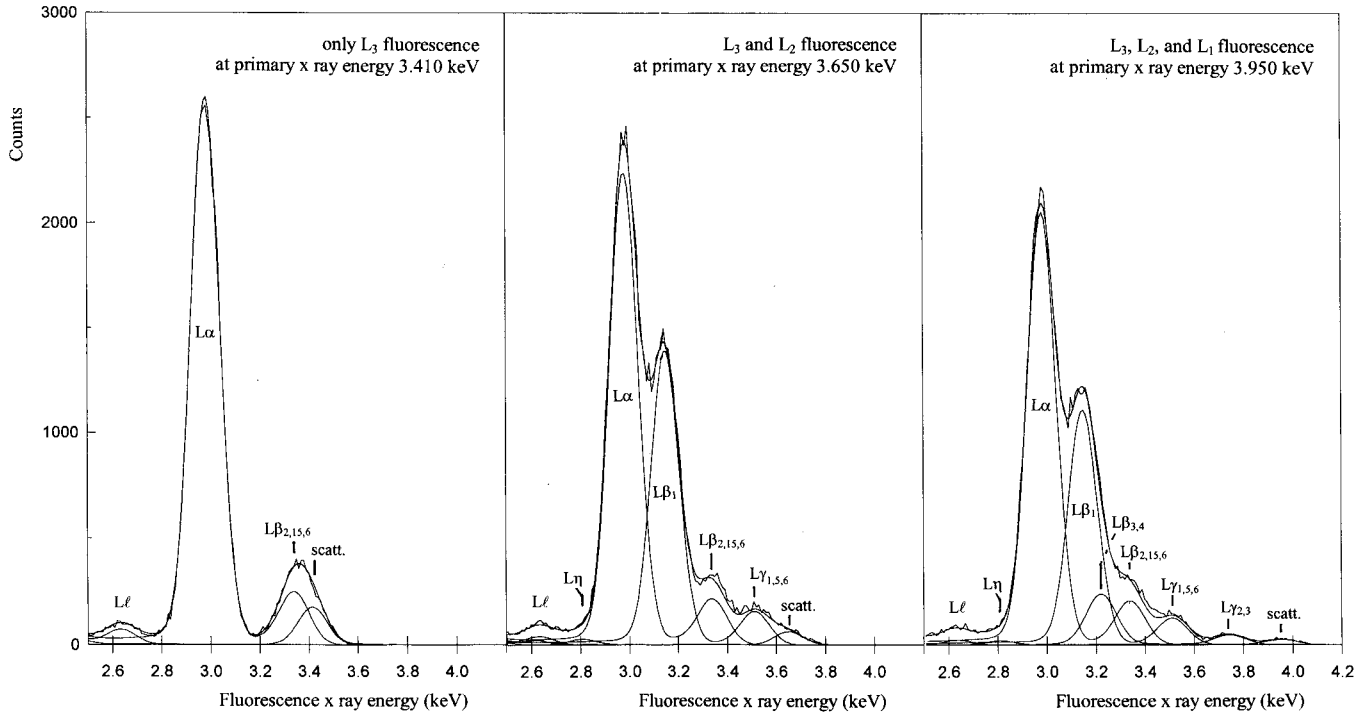

FIG. 1. Recorded fluorescence spectra and fitted lines. The peak ''scatt.'' originates from elastic scattering and occurs at the primary x-ray energy.

modest accuracy were available.

About a decade ago, we have pioneered a new experimental method for measuring vacancy yields employing monochromatized tunable synchrotron radiation [8]. This method makes use of the fact that the ionization of a particular subshell can be switched on or off by tuning the incident photon energy across the respective ionization threshold. Either the induced x-ray fluorescence or the Auger electrons are detected. This experimental method can provide yields of all L subshells. The achieved accuracy is good, since it is a direct method and the photoionization cross sections are rather well known both from theoretical calculations as well as from experimental mass attenuation data. Various investigations by this method have been performed in recent years (in chronological order): (i) by fluorescence detection; $Z=79$ [8], $Z=72-82$ [9], $Z=62$ [10], and $Z=54$ [11], and (ii) by Auger-electron detection; $Z=39$ [12], $Z=47$ [13], and $Z=28,28,42$ [14].

As outlined above, measurements of L subshell yields at $Z\approx 49$ are of particular interest to study the cutoff of the strong L_1-$L_3M_{4,5}$ Auger channel. The Coster-Kronig yields of $_{47}$Ag have been previously studied via the detection of Auger electrons [13]. This measurement, however, suffers from main experimental problems:

(a) The counting statistics is poor since both the production of Auger electrons in the interesting thin surface layer and the detection via an electron spectrometer are inefficient. Furthermore, there is considerable background in the spectra (electrons from the depth of the solid target), which introduces noise. Due to the poor counting statistics, the derived vacancy yields bear substantial statistical uncertainty. Furthermore, a change of background may introduce systematic errors. The spectra shown in Ref. [13] suggest a reasonable quality of the data. However, these are not the original recorded spectra but that after background subtraction and smoothing.

(b) The Auger spectrum consists of a large number of individual lines. In order to extract the contributions originating from individual L subshells, a massive theoretical input on positions and strengths of lines is required. Since this input bears some uncertainty, also the extracted results may suffer from systematic problems.

(c) Due to the weak signal, measurements were taken at only three primary photon energies. In the data evaluation, simply the ionization cross at these energies as predicted by single-electron calculations were taken. However, meanwhile it has been recognized that electron correlation effects significantly affect the ionization cross sections and thus the derived Coster-Kronig yields.

Reference [13] states rather small uncertainties of the obtained Coster-Kronig yields, e.g., $f_{12}=0.044\pm 0.004$. Since the L_1 ionization cross section is about half as large as the L_2 ionization cross section, this f_{12} value means that the intensity of L_2 Auger electrons actually increases by ca. 2.2% $\pm 0.2\%$ when the primary photon energy is tuned above the L_1 edge. The stated uncertainty must be judged as much too small regarding the statistical and systematical uncertainties of this experiment.

In order to obtain decisive values of the Coster-Kronig yields of $_{47}$Ag we decided to perform a measurement making use of the induced fluorescence. The detection of fluorescence is advantageous as compared to the detection of Auger electrons: X rays are produced rather efficiently and can be detected efficiently and energy dispersive by a Si (Li) detector. Thus very good statistics is obtained within reasonable measuring times at present synchrotron facilities even if the

TABLE I. Values of x-ray lines used as input in the spectra fit.

	Energy of x-ray line (Ref. [20]) (eV)	Relative contribution to radiative decay (Ref. [22])	Natural Lorentzian width of line (Ref. [21]) (eV)
Al K fluorescence			
$K\alpha$	1.486.6	–	–
Ag L_3 fluorescence			
Ll	2 633.7	3.3%	10.8
$L\alpha_1$	2 984.3	79.1%	2.4
$L\alpha_2$	2 978.2	8.9%	2.4
$L\beta_6$	3 256.0	0.6%	2.4
$L\beta_{2.15}$	3 347.8	8.0%	2.4
Ag L_2 fluorescence			
$L\eta$	2 806.1	2.6%	11
$L\beta_1$	3 150.9	88.5%	2.6
$L\gamma_5$	3 428.3	0.5%	2.6
$L\gamma_1$	3 519.6	8.3%	2.6
Ag L_1 fluorescence			
$L\beta_3$	3 234.5	52.0%	6.7
$L\beta_4$	3 203.5	31.2%	6.7
$L\beta_9$	3 439.2	0.5%	6.7
$L\beta_{10}$	3 432.9	0.3%	6.7
$L\gamma_2$	3 743.2	5.6%	12
$L\gamma_3$	3 749.8	9.4%	12

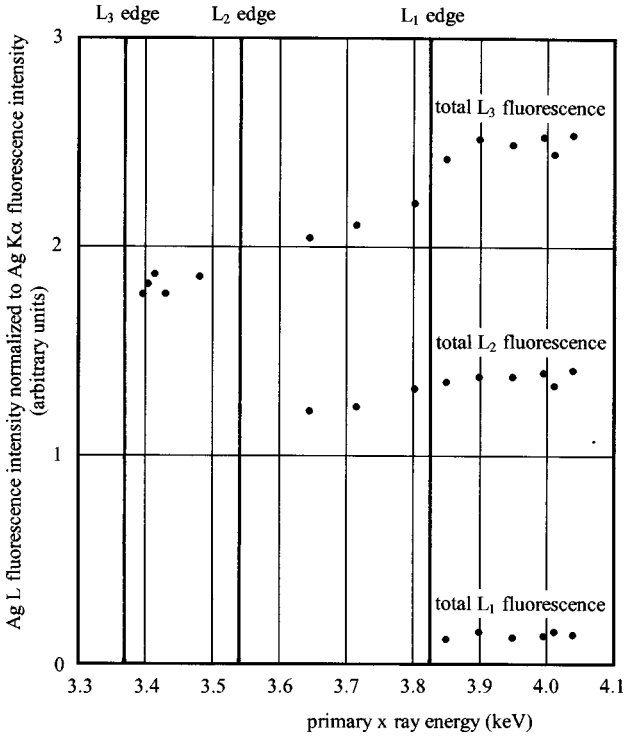

FIG. 2. Total intensities of the fluorescence of a particular Ag L_i subshell normalized to the simultaneously recorded Al $K\alpha$ line versus primary photon energy.

fluorescence yield amounts to a few percent only. Furthermore, the x-ray spectra are less complex than the Auger electron spectra, which facilitates the data analysis. There is some line overlap in the recorded L fluorescence spectra of intermediate-Z elements due to the limited energy resolution of the Si (Li) detector. Since positions and strengths of the lines are well known both from crystal-spectrometer measurements and theoretical calculations, an extraction of the contributions originating from individual subshells can be reliably performed by careful data fitting as shown in our previous measurements on $_{54}$Xe [11].

Measurements on decay yields through synchrotron photoionization require reliable photoionization cross sections. Although the cross sections vary rather smoothly with energy, a specific structure in the regime of the absorption edges exists. This structure results from electron correlation effects and amounts to a few percent. It is small, but directly affects the extraction of Coster-Kronig yields from the measured intensity jumps at the edges. Due to their importance, we have previously studied the structure both experimentally and theoretically for large-Z [15] and intermediate-Z elements [16].

The detection of the induced x-ray fluorescence offers the possibility to extract *all L* subshell yields: The Coster-Kronig yields are derived from intensity jumps at the absorption edges, the fluorescence yields are derived from the absolute intensities of x-ray lines, and the Auger yields are obtained from the normalization of all yields of a particular subshell to unity. In contrast, Auger measurements provide no information on the fluorescence yields when these are small (i.e., less than a few percent).

II. EXPERIMENT

The measurements were performed at the x-ray beam line at the electron storage ring Elektronenspeicheranlage (ELSA) in Bonn. The synchrotron radiation is monochromatized by a double-crystal spectrometer and then delivered to the apparatus. The experimental setup is similar to the one used in previous works [10,11]. The primary radiation hits the target that is tilted by 45° towards the incoming beam. The induced x-ray fluorescence is detected by a Si (Li) detector located at 90° towards the incoming beam. Since scattering of primary radiation (e.g., by air) into the detector disturbs the recorded spectra, the path of the primary beam and the target were surrounded by a vacuum tube. Only minor scattering by the target itself remains. The target consists of two foils: Ag as an element under investigation and Al whose $K\alpha$ radiation is used for normalization purposes. The foils were delivered by the Goodfellow company specified as 1-μm Ag and 0.8-μm Al, each evaporated on a thin plastic support foil.

Fluorescence spectra were recorded with monochromator settings in the energy range from 3.4 (just above the $_{47}$AgL_3 edge) to 4.9 keV (well above all $_{47}$AgL edges). Figure 1 shows some typical spectra recorded at different primary energies. The actual energy of the primary radiation was checked from the fluorescence spectra, which contain a small amount of primary radiation. The deviations between nominal and actual primary energy were small, typically a few eV, which is in the order of the fitting accuracy. Harmonics in the primary beam were not present since the synchrotron radiation of ELSA drops sharply at energies above a few keV. In fact, the recorded fluorescence spectra give no indication of ionization of a $_{47}$AgL subshell at a primary radia-

TABLE II. Analytical fit to the calculated photoelectric cross section [24].

Ionized shell	Fitted function of ionization cross section
$_{47}$Ag, L_3 subshell	3.167 Mb $(E/\text{keV})^{-2.4733}$
$_{47}$Ag, L_2 subshell	1.509 Mb $(E/\text{keV})^{-2.3802}$
$_{47}$Ag, L_1 subshell	0.285 Mb $(E/\text{keV})^{-1.6009}$
$_{13}$Al, K shell	0.644 Mb $(E/\text{keV})^{-2.7162}$

tion below its absorption edge caused by harmonics.

The various $_{47}$Ag x-ray lines in the recorded spectra show considerable overlap which results both from the number of lines each having a natural width and from the finite resolution of the Si (Li) detector. In order to extract the true line intensities without systematic errors, an advanced fitting procedure with an accurate modeling of the actual line shape is required [17,11,18]. In the present case, the excitation by tunable primary energy bears advantages: For example, when only the L_3 subshell is ionized, the spectra only have L_3 x rays, which are reasonably well resolved to establish the experimental parameters for the fit. For that reason, the spectra were analyzed in successive steps, i.e., first only L_3 fluorescence, then L_3 and L_2 fluorescence, etc, using the computer program GPPFNC [19]. Individual x-ray peaks were represented by a Lorentzian profile, which was convoluted with the detector response represented by the Hypermet function [18]. This function contains a Gaussian function, an exponential tail and a flat plateau stretching the range from zero energy to the x-ray peak. The two latter contributions originate from incomplete charge collection in the detector. There were four ranges for the tail parameters (boundaries at 0, 1.8, 2.7, 3.6, and 10 keV) and within each range the parameters were kept to be the same. The parameters of the exponential tail and the plateau were determined successively from the spectra of Al K and Ag L x rays.

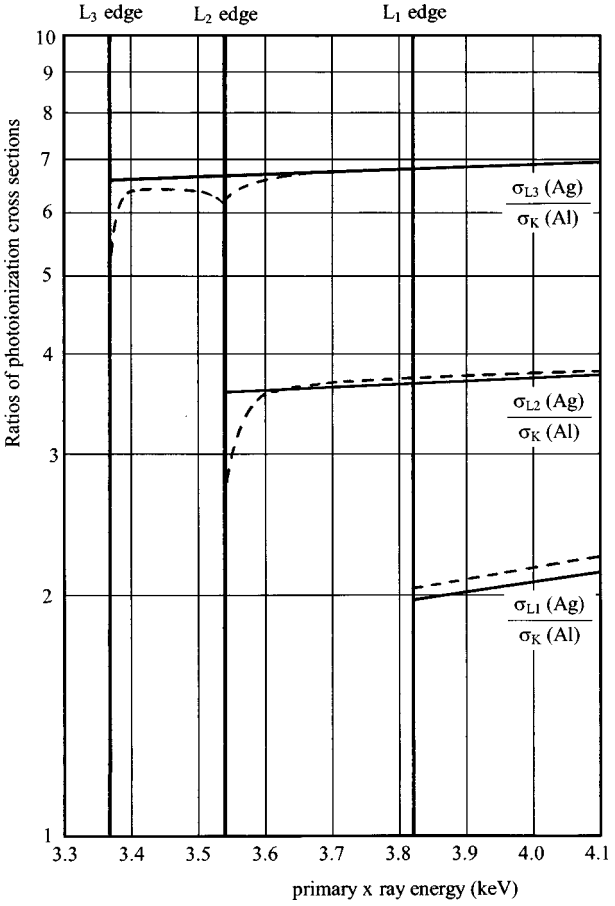

FIG. 3. Ratios of theoretical photoelectric cross sections. Data for the Al K shell were taken from relativistic Hartree-Slater calculations (RHS) by Scofield [24]. Data for Ag L_i subshells were taken also from RHS (solid curve) and from the LRA by Doolen (cited in Ref. [16]) (dashed curve).

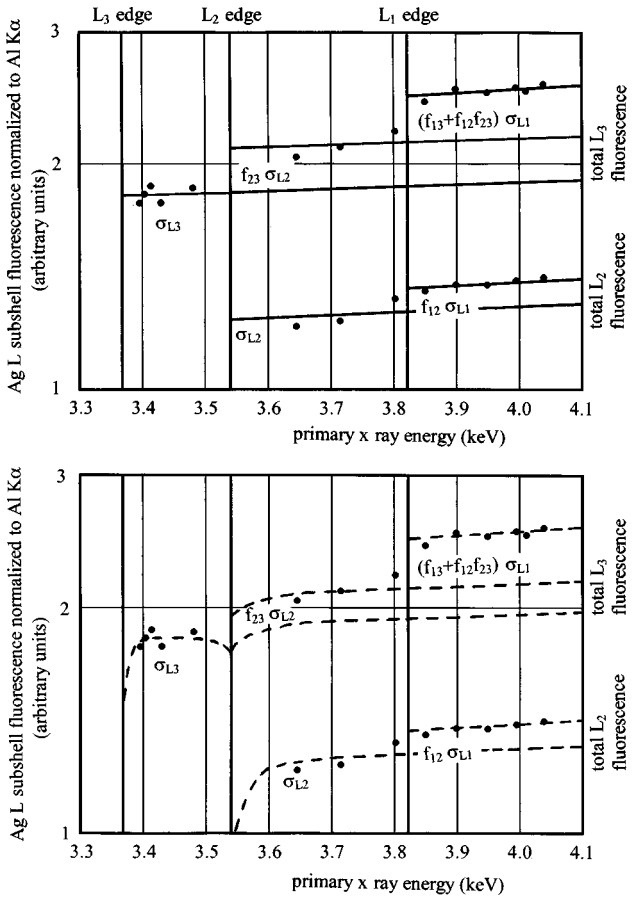

FIG. 4. Experimentally measured L_3 and L_2 subshell normalized fluorescence (dots) and fitted curves using the ionization cross section ratios shown in Fig. 3. Top (solid curve): RHS. Bottom (dashed curve): LRA.

The spectra have three series of x-ray lines, corresponding to the three Ag L subshells. In each series there is a strong line (i.e., $L\alpha$, $L\beta_1$, and $L\beta_{3,4}$, respectively) and usually many weaker lines (Table I). In the analysis of the spectra, the weak lines were locked to the main line within each series by assigning their positions, intensities, and widths. The positions were calculated using tabulated energies [20]. The natural widths were taken from tabulations [21]. Their intensities were kept fixed to the main line, the ratios of the intensities were assumed to be that of Dirac-Fock calculations [22] and were corrected for the detector efficiency. Each series had two groups. The L_3 x rays were fitted as the individual Ll and $L\alpha$ lines, and the intensities of all the other L_3 x rays were locked to the $L\alpha$ line. Similarly, the L_2 x rays

TABLE III. Coster-Kronig yields of $_{47}$Ag. Values of the present paper have been obtained by fitting measured fluorescence intensities to calculated cross sections, either by RHS (electron correlations not included), which are not regarded as reliable, and by LRA (electron correlations included).

	f_{23}	f_{12}	f_{13}
Theory (1981) [1]	0.155	0.068	0.740
Semiempirical (1979) [26]	0.15±0.03	0.10±0.02	0.59±0.06
Experiment (1989) [13]	0.16±0.03	0.044±0.004	0.61±0.05
Present experiment, using RHS	0.27	0.14	0.58
Present experiment, using LRA	0.18±0.03	0.14±0.03	0.58±0.05

were split into $L\eta$ and $L\beta_1$, and the other L_2 x rays were locked to the $L\beta_1$ line. In contrast, the L_1 series was divided in the $L\gamma_{2,3}$, $L\beta_3$, $L\beta_4$, and $L\beta_{9,10}$ groups. Additionally, for the strong $L\alpha$ and $L\beta_2$ lines each a satellite line was fitted with the same intensity ratios as the corresponding diagram line ratios and with an energy 33 eV above the diagram lines as follows from calculations [23]. The inclusion of satellites adds one additional variable to the fit.

III. EXTRACTION OF YIELDS

The derived line intensities were not corrected for absorption of the primary radiation and the emitted fluorescence inside the target foils. This correction may either increase or decrease the ratio of Ag L x rays and Al K x rays line intensities, depending on the mounting sequence of the Ag and Al foils. Unfortunately, the mounting positions during the experiment were not documented. The effect on the derived fluorescence yields turns out to be almost negligible as compared to the other error sources. More crucial is the correction in the case of Coster-Kronig yields. Since the mounting positions were not changed during the experiment, also here the correction has almost a negligible effect on the derived results.

Figure 2 shows the measured total Ag L_3, Ag L_2, and Ag L_1 fluorescence intensities normalized to the Al $K\alpha$ line at different primary energies. The fluorescence from a particular Ag L subshell originates both from direct ionization of the subshell as well as vacancy transfer from deeper lying subshells by Coster-Kronig transitions. Let $I_{\mathrm{Li}}(E)$ denote the total fluorescence intensity of the Ag L_i subshell and I_K that of the Al $K\alpha$ line, excited by primary radiation at energy E. Then the normalized Ag L_i fluorescence can be described by the following expressions:

$$\frac{I_{L1}(E)}{I_K(E)} = C\omega_1 \frac{\sigma_{L1}(E)}{\sigma_K(E)}, \tag{1}$$

$$\frac{I_{L2}(E)}{I_K(E)} = C\omega_2 \left[\frac{\sigma_{L2}(E)}{\sigma_K(E)} + f_{12}\frac{\sigma_{L1}(E)}{\sigma_K(E)} \right], \tag{2}$$

$$\frac{I_{L3}(E)}{I_K(E)} = C\omega_3 \left[\frac{\sigma_{L3}(E)}{\sigma_K(E)} + f_{23}\frac{\sigma_{L2}(E)}{\sigma_K(E)} + (f_{13} + f_{12}\cdot f_{23})\frac{\sigma_{L1}(E)}{\sigma_K(E)} \right]. \tag{3}$$

Here, C is an instrumental constant. The above formulae are valid for all energies E if one puts $\sigma_{\mathrm{Li}}=0$ at energies below the corresponding ionization threshold.

Since ionization cross sections vary rather smoothly with energy except at the edges, the fluorescence intensities are also expected to vary smoothly. The experimental points in Fig. 2 exhibit some scatter, which is larger then expected from the counting statistics (~1%, approximate size of the dots). Possibly, the scatter results from minor fluctuations of the position of the primary beam. As expected, the fluorescence intensities exhibit jumps at the absorption edges due to the creation of additional vacancies by vacancy transfer from deeper lying subshells by Coster-Kronig transitions.

In order to extract the Coster-Kronig yields from the measured intensities, the measured fluorescence intensities have to be matched to the ionization cross sections according to the ansatz of Eqs. (2) and (3), whereby the Coster-Kronig yields are fitting parameters. For this purpose, the ionization cross section ratios Ag σ_{Li} to Al σ_K are required. In a first trial, we used the advanced theoretical cross sections obtained by a relativistic treatment of the ionization process and employed a relativistic Hartree-Slater potential (RHS) [24]. The theoretical values are tabulated at some energies and are known to exhibit a smooth behavior. For convenience, the tabulated values were interpolated by analytical functions as given in Table II. Figure 3 shows the obtained cross-section ratios versus primary energy. The fit of the measured fluorescence intensities to the cross-section ratios

TABLE IV. Fluorescence yields of the $_{47}$Ag L subshells. The * denotes the value adopted in the present paper (average of the values given in Refs. [1, 25, 26]).

	ω_1	ω_2	ω_3
Theoretical (1981) [1]	0.0114	0.056	0.0577
Semiempirical (1979) [26]	0.016±0.004	0.051±0.010	0.052±0.008
Experimental (1988) [25]	0.016±0.003	0.055±0.009	0.058±0.010
Present experiment, using LRA	0.013±0.002	0.067±0.009	0.056±0.007*

TABLE V. Auger yields of the $_{47}$Ag L subshells.

	a_1	a_2	a_3
Theoretical (1981) [1]	0.181	0.789	0.942
Semiempirical (1979) [26]	0.29±0.08	0.80±0.04	0.948±0.008
Present paper	0.27±0.08	0.75±0.04	0.944±0.007

is shown in Fig. 4, top. In the figure, the correspondence between a particular jump and the corresponding Coster-Kronig yield is indicated.

Although this data fit looks reasonable, it gives wrong results due to the minor errors in the ionization cross sections. In order to extract the jump ratios, the precise dependence of ionization cross sections on primary energy plays a crucial role. As follows from our previous studies, the actual cross sections exhibit minor characteristic deviations from the predictions of the RHS calculations, which originate from electron correlation effects [15]. The collective response of all atomic electrons to the external field basically causes a screening of the field, which can be treated in a linear response approximation (LRA). Our studies on the electron correlations by mass attenuation measurements and comparative LRA calculations have clearly established these effects and have shown that the LRA model qualitatively well reproduces the features but somewhat overestimates their size [16]. According to these studies, the ionization cross sections of the Ag L_i subshells should be corrected for the electron correlation effects. Since these correlation effects are pronounced mainly in the vicinity of the absorption edges, no correction of the ionization cross section of Al K is required. Figure 3 also shows the corrected ratios of ionization cross sections.

As second trial of the data evaluation, the experimental fluorescence intensities (Fig. 2) were fitted to the corrected ratios of ionization cross sections (Fig. 3). It is felt that this fit is the best which can be done. Furthermore, data points in the immediate vicinity of the L_i edges were not considered since here the correlation effects are strongest and also other disturbances by the edge structure occur (e.g., extended x-ray absorption fine structure). The obtained fit is shown in Fig. 4, bottom.

The Coster-Kronig yields obtained by both fits are shown in Table III. Comparing the first fit to the second, the main difference occurs in the f_{23} value. This difference can be traced back to the different energy dependencies of the ionization cross section σ_{L3} in the RHS and LRA calculations. As already stated, the second fit is believed to be reliable. This result is corroborated by the fact that the f_{23} value obtained in the second fit (LRA) agrees well with other published data (Table III), whereas the f_{23} value obtained in the first fit (RHS) significantly disagrees. The results for f_{12} and f_{13} are the same in both fits, which might be fortuitous.

The applied method allows—in principle—an absolute measurement of the individual L subshell fluorescence yields: When the energy of the primary radiation is tuned from below to above an absorption edge, the absorption of primary photons abruptly increases. Simultaneously, the fluorescence originating from the corresponding subshells is excited. Comparing the number of additionally adsorbed photons and the emitted fluorescence photons directly provides the fluorescence yield. Such an experiment, however, would require a tedious absolute calibration of the detectors for the absorbed and emitted fluorescence photons.

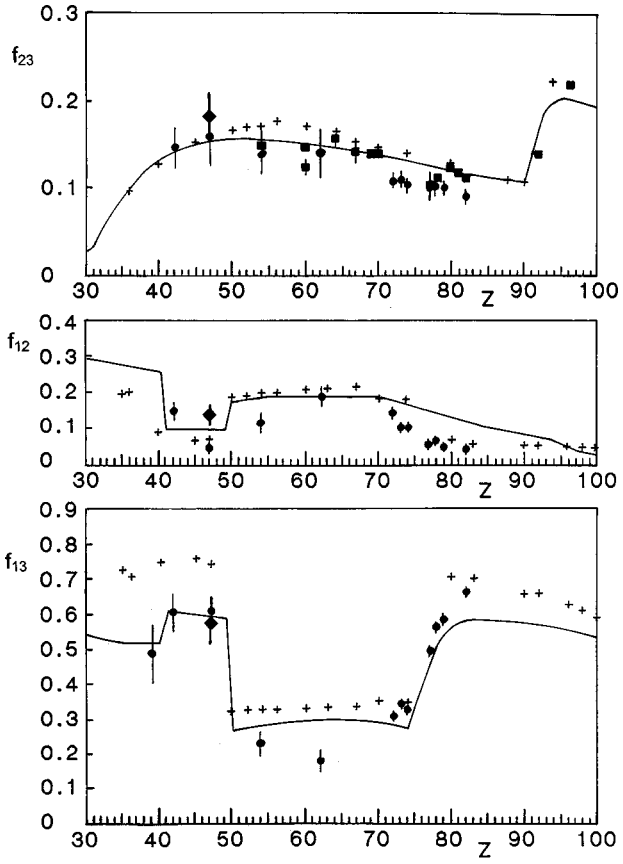

FIG. 5. Compilation of L-subshell Coster-Kronig yields for all elements (taken from Ref. [11] with new data added). Crosses (+) are theoretical results [1], curve is the semiempirical fit [26], squares (■) are experimental results obtained by the $K\alpha$-$L\alpha$ coincidence method, dots (●) are experimental results obtained by the synchrotron photoionization method, and diamonds (◆) are results of the present paper.

On the other hand, the fluorescence yield ω_3 is rather well known. Then it is straightforward from our experiment to derive the fluorescence yields ω_1 and ω_2. The Si Li detector used for the fluorescence detection has a detection efficiency close to unity, a slight decrease towards smaller energies of the fluorescence can be corrected using the efficiency curve supplied by the manufacturer. With this correction, the fluorescence intensities of all three Ag L_i subshells are obtained with equal efficiencies, i.e., the constant C in Eqs. (1)–(3) is indeed the same in all three equations as already tacitly assumed.

We adopt $\omega_3=0.056\pm0.007$ from other work (see compilation in Table IV). Matching the measured fluorescence (Fig. 2) to the LRA ionization cross sections, the fluorescence yields ω_1 and ω_2 are obtained. Our results compare well with other experimental and theoretical data (Table IV).

Finally, the Auger yields are derived from the normalization of all yields to unity:

$$a_3=1-\omega_3, \tag{4}$$

$$a_2 = 1 - \omega_2 - f_{23}, \quad (5)$$

$$a_1 = 1 - \omega_1 - f_{12} - f_{13}. \quad (6)$$

The obtained results are given and compiled to other data in Table V.

IV. DISCUSSION

A comprehensive collection of *L*-subshell Coster-Kronig yields for all elements is shown in Fig. 5. The present results for f_{23} and f_{13} of $_{47}$Ag fit nicely to the body of data.

Regarding the present result for f_{12} of $_{47}$Ag it is about three times larger than that obtained in an earlier experiment [13]. It should be noted that in this earlier experiment the Auger electrons were detected, which causes various problems as discussed in the introduction of the present paper. Interestingly, the present result for f_{12} of $_{47}$Ag is in accordance with the f_{12} value of the neighboring element $_{42}$Mo obtained by another earlier experiment by the same group using the same technique [14].

The various measurements of *L*-subshell yields performed in the last decade have demonstrated that this method is a powerful tool for determining yields of the inner-shell decay. Experimentally, the detection of the fluorescence emitted in the vacancy decay is advantageous as compared to the detection of Auger electrons. So far, the fluorescence has been detected by semiconductor detectors. These detectors provide high-detection efficiency but the resolution is modest for the present application. Measurements of the *L*-subshell fluorescence provide no problem in case of large-*Z* elements. In case of intermediate-*Z* elements, a sophisticated spectrum analysis is required, as was demonstrated in the present experiment.

With the advent of very brilliant synchrotron light sources it seems feasible to employ other detector types such as crystal spectrometers or cryobolometers, which offer higher resolution at the expense of efficiency. Using these detectors, the *L* subshells of small-*Z* elements as well as the *M* subshells of intermediate-*Z* and large-*Z* elements seem accessible. This would open a wide field of experimental studies on these challenging systems, where reliable experimental data so far are almost nonexistent, and provide the basis for decisive studies of a wide variety of processes in the decay of inner-shell vacancies and their interplay.

ACKNOWLEDGMENTS

M. Bonerath was engaged in the measurements. The generous support by Professor Dr. J. Hormes and the ELSA staff is gratefully acknowledged.

[1] M. H. Chen, B. Crasemann, and H. Mark, Phys. Rev. A **24**, 177 (1981).
[2] M. H. Chen, B. Crasemann, K.-N. Huang, M. Aoyagi, and H. Mark, At. Data Nucl. Data Tables **19**, 97 (1977).
[3] S. Puri, D. Mehta, B. Chand, N. Singh, and P. N. Trehan, X-Ray Spectrom. **22**, 358 (1993).
[4] B. L. Doyle and S. M. Shafroth, Phys. Rev. A **19**, 1433 (1979).
[5] E. Rosato, Nucl. Instrum. Methods Phys. Res. B **15**, 591 (1986); J. Q. Xu and E. Rosato, *ibid.* **33**, 297 (1988).
[6] P. V. Rao, in *Atomic Inner-Shell Processes*, edited by B. Crasemann (Academic, New York, 1975), Vol. II, p. 1.
[7] W. Jitschin, in *X-Ray and Inner-Shell Processes*, edited by T. A. Carlson, M. O. Krause, and S. T. Manson, AIP Conf. Proc. No. 215 (AIP, New York, 1990), p. 408.
[8] W. Jitschin, G. Materlik, U. Werner, and P. Funke, J. Phys. B **18**, 1139 (1985).
[9] U. Werner and W. Jitschin, Phys. Rev. A **38**, 4009 (1988).
[10] R. Stötzel, U. Werner, M. Sarkar, and W. Jitschin, Phys. Rev. A **45**, 2093 (1992); J. Phys. B **25**, 2295 (1992).
[11] W. Jitschin, R. Stötzel, T. Papp, M. Sarkar, and G. D. Doolen, Phys. Rev. A **52**, 977 (1995).
[12] W. Jitschin, G. Grosse, and P. Röhl, Phys. Rev. A **39**, 103 (1989).
[13] S. L. Sorensen, R. Carr, S. J. Schaphorst, S. B. Whitfield, and B. Crasemann, Phys. Rev. A **39**, 6241 (1989).
[14] S. L. Sorensen, S. J. Schaphorst, S. B. Whitfield, B. Crasemann, and R. Carr, Phys. Rev. A **44**, 350 (1991).
[15] W. Jitschin, U. Werner, G. Materlik, and G. D. Doolen, Phys. Rev. A **35**, 5038 (1987).
[16] W. Jitschin and R. Stötzel, Phys. Rev. A **58**, 1221 (1998).
[17] T. Papp, J. L. Campbell, and S. Raman, Phys. Rev. A **49**, 729 (1994).
[18] T. Papp and J. L. Campbell, Nucl. Instrum. Methods Phys. Res. B **114**, 225 (1996).
[19] J. A. Maxwell, J. L. Campbell, and W. J. Teesdale, Nucl. Instrum. Methods Phys. Res. B **43**, 218 (1989).
[20] J. A. Bearden, Rev. Mod. Phys. **39**, 78 (1967).
[21] O. Keski-Rahkonen and M. O. Krause, At. Data Nucl. Data Tables **14**, 139 (1974).
[22] J. H. Scofield, At. Data Nucl. Data Tables **14**, 121 (1974); Phys. Rev. A **10**, 1507 (1974); **12**, 345(E) (1975).
[23] M. H. Chen, B. Crasemann, M. Aoyagi, and H. Mark, Phys. Rev. A **15**, 2312 (1977).
[24] J. H. Scofield (unpublished).
[25] J. Auerhammer, H. Genz, and A. Richter, Z. Phys. D **7**, 301 (1988).
[26] M. O. Krause, J. Phys. Chem. Ref. Data **8**, 307 (1979).